4.6 SURVEY, ALIGNMENT, AND GEODESY (WBS 1.1.6)

4.6.1 Introduction

For a long baseline neutrino experiment, properly aligning the neutrino beam to hit the far detector 735 km away is clearly important. Actually, as shown in **Figure 4.6-1**, the NuMI beam, for low neutrino energies, is several kilometers wide and modern geodetic survey techniques, especially the Global Positioning System (GPS) satellites, make hitting the far detector relatively straightforward. For the NuMI beamline, the physics-driven alignment goals from the MINOS experiment require that the neutrino beam center must be within 100 meters of the far detector.

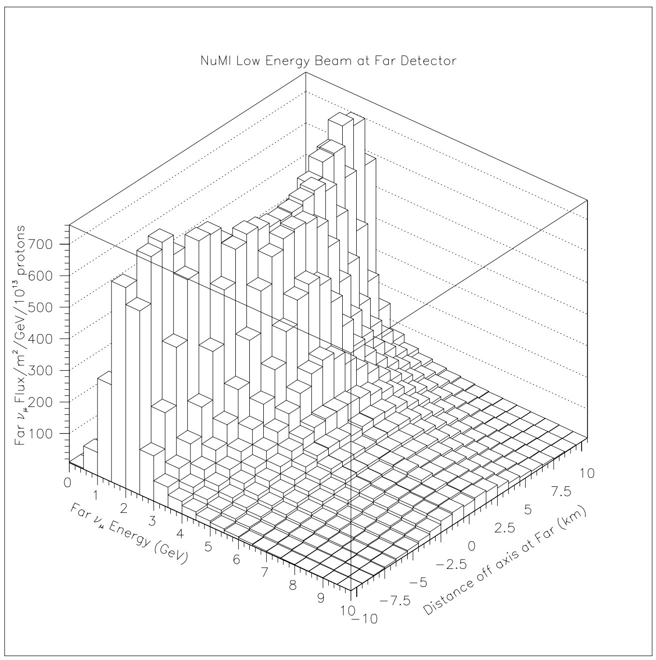

Figure 4.6-1 Transverse distribution of the NuMI low energy tune neutrino beam at the far detector as a function of energy. Note that at low neutrino energy the beam is several kilometers wide

4.6.2 System Description: Determining the Line from Fermilab to Soudan

The relative positions of Fermilab and Soudan on the surface are determined by making simultaneous measurements using the Global Positioning System (GPS) satellites. Simultaneous GPS data at both Fermilab and Soudan were recorded in April 1999 as shown in **Table 4.6-1**. The data was analyzed at Fermilab and, independently, by the National Geodetic Survey (NGS). The agreement between the NGS result and two methods of analysis at Fermilab was excellent. The Fermilab to Soudan vector, averaged over the period of the observations used, is known to better than 1 cm horizontally and 6 cm vertically, well within requirements. The differential earth tide effect between Fermilab and Soudan is approximately the same as this uncertainty.

Included in **Table 4.6-1** are the results from two less precise measurements also using professional GPS receivers, which agree to better than 1 meter, and a later result using an amateur hand held receiver. All four results are within the 12-meter tolerance goal for this measurement. Accuracy of a differential GPS measurement is increased by including CORS (Continuously Observed Reference Station) data in the analysis (**Figure 4.6-2**), simultaneous observations from both positions, and using the precise satellite positions calculated by NGS from the CORS data.

Year	Receiver	Measure time (hour)	Include CORS	Simulta-neous	Precision Satellite Positions	Deviation from 1999 (meter)
1999	Professional	26	Yes	Yes	Yes	
1998	Professional	6	No	Yes	No	0.231
1994	Professional	1	No	No	No	0.785
2000	Hand held	<1	No	No	No	10.140

Year			Azimuth			Vertical	Distance (meter)	north (meter)	east (meter)	up (meter)	$\|(\delta n,\delta e,\delta u)\|$ (meter)
1999	336	5	52.383	-3	17	17.882	735273.058	671108.532	-297424.016	-42175.390	
1998			-0.033			-0.008	-0.196	-0.229	-0.029	-0.018	0.231
1994			-0.007			0.001	-0.785	-0.725	0.296	0.049	0.785
2000			0.654			2.278	5.608	6.487	-0.330	7.787	10.140

Table 4.6-1. Relative position of the SHAFT monument on the surface at Soudan as measured from Fermilab surface monument 66589 by GPS. Results are given in the Local Geodetic Coordinate System (reference SHAFT). The values for the most accurate measurement are given on the first line, followed by the differences (other – best) of the three additional measurements relative to the best one. The professional receivers used were Trimble 4000 SSi's; the hand held receiver was a Garmin GPS III+ (Best Buy ~$350).

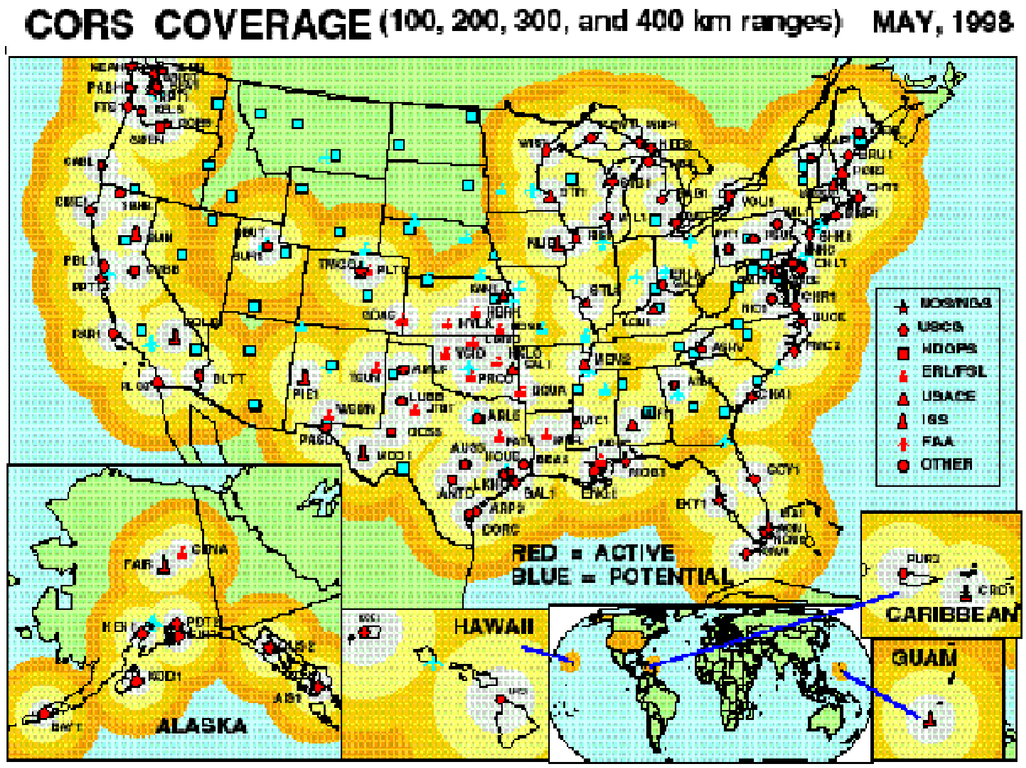

Figure 4.6-2 CORS (Continuously Observed Reference Station) network. GPS data are recorded for over 100 accurately known locations in the United States, including 4 in Wisconsin. (Source: National Geodetic Survey www page: http://www.ngs.noaa.gov/CORS/Maps.html

The position of the 27th level at the bottom of the Soudan Mine, relative to the surface, is determined using inertial survey. An inertial survey unit and operator were rented from the University of Calgary during the April 1999 GPS trip to Soudan. The inertial survey unit used (Honeywell Laseref III IMU) contains a triad of accelerometers and optical gyroscopes to measure force and angular velocity. The accelerometers are double integrated to yield position change along each of the 3 axes. Internal consistency of the several inertial survey runs indicated a 0.7 m per coordinate precision for the surface to bottom of the mine measurement, many times better than the 12 m goal. As shown in **Table 4.6-2,** these measurements agreed to better than 4 m per coordinate with the old mine values for the 27th level relative to the surface.

	east	north	up
	meter	meter	meter
1999 INS values	-15.2	148.2	-710.1
INS-old mine #'s	-0.2	3.7	-3.4

Table 4.6-2. Inertial Survey (INS) measurement from the surface to level 27 at Soudan. The average of the 4 INS runs made on April 20, 1999 is given, together with the change of these measurements from the old mine values.

Conventional survey techniques are used to determine the position of the MINOS far detector relative to the bottom of the shaft at Soudan. **Table 4.6-3** gives the position of monuments in the MINOS cavern and the nominal detector axis and edges in the Cartesian Local Geodetic Coordinate System (LGCS) relative to the surface monument called "SHAFT" (which was used in the surface GPS measurement above). **Table 4.6-4** gives the same points in the Cartesian beam coordinate system, with origin at the nominal detector center, Y axis along the neutrino beam direction, and X axis horizontal.

POINT NAME	X(+EAST) (Meter)	Y(+NORTH) (Meter)	Z(+UP) (Meter)
BRASS_1	37.3668	10.8767	-709.1782
BRASS_2	32.5269	20.5614	-709.1638
BRASS_3	24.9370	35.7484	-709.1476
BRASS_4	17.9893	49.6496	-709.1606
BRASS_5	3.3012	79.0429	-709.1639
CP_E11	27.1329	39.8453	-705.0098
CP_E14	24.6850	44.7639	-705.0327
CP_E17	22.2376	49.6672	-705.0330
CP_E2	34.2510	25.6183	-705.0434
CP_E5	31.7950	30.5282	-705.0347
CP_E8	29.3449	35.4377	-705.0233
CP_W11	19.5038	36.0554	-705.0210
CP_W14	17.0549	40.9669	-705.0257
CP_W17	14.6069	45.8628	-705.0210
CP_W2	26.6014	21.8538	-705.0311
CP_W5	24.1563	26.7486	-705.0431
CP_W8	21.7098	31.6510	-705.0386
EI_01	34.1657	23.6082	-709.2540
EI_035	31.8929	28.1608	-709.2580
EI_065	29.5962	32.7045	-709.2534
EI_10	27.2189	37.4801	-709.2451
EI_125	24.9455	42.0243	-709.2487
EI_155	22.6748	46.5704	-709.2416
EI_18	20.5332	50.8897	-709.2587
EO_01	37.0840	23.7565	-709.2491
EO_09	29.9725	38.0342	-709.2452
EO_19	21.3997	54.7230	-709.2630
PP1	8.2536	51.7757	-707.5768
PP2	4.2885	59.6857	-707.5483
PP3	1.1212	66.0377	-707.5610
VULCAN_E	31.7687	30.2899	-707.0321
VULCAN_W	24.2997	26.7597	-706.8035
WBE_1	17.6527	55.4088	-709.2568
WBE_1_5	16.7981	60.6413	-709.2508
WBE_2	13.3126	64.1350	-709.2516
WBE_2_5	11.7837	70.7375	-709.2529
WBE_3	8.2340	74.4346	-709.2519
WBW_1	10.6467	51.9149	-709.2533
WBW_1_5	7.8540	55.7006	-709.2597
WBW_1_7	7.2439	59.4027	-709.2612
WBW_2	6.2549	60.6034	-709.2562
WBW_2_2	5.2874	63.5825	-709.2643
WBW_2_5	2.4974	66.3988	-709.2517
WBW_3	1.1941	70.8040	-709.2534
WI_01	28.3010	20.6410	-709.2532
WI_035	26.0234	25.2087	-709.2504
WI_065	23.7625	29.7489	-709.2521
WI_10	21.3667	34.5228	-709.2503
WI_125	19.1039	39.0775	-709.2530
WI_155	16.8175	43.6237	-709.2527
WI_18	14.6497	47.9674	-709.2615
WO_01	26.9941	18.7946	-709.2483
WO_09	19.8536	32.9234	-709.2434
WO_185	12.3356	47.9075	-709.2598
DetCtr_dsgn	24.4433	35.7132	-704.5203
DetCtr_meas	24.3847	35.8303	-704.5203
dcs_origin	31.3726	21.8483	-704.5203
FD_ds_axis	17.3968	49.8124	-704.5203
FD_us_right	34.9506	23.6365	-704.5203
FD_us_left	27.7946	20.0601	-704.5203
FD_us_top	31.3726	21.8483	-700.5203
FD_us_bot	31.3726	21.8483	-708.5203
FD_us_t,r	34.9506	23.6365	-700.5203

Table 4.6-3. Far Cavern Monuments and Detector Points in the Local Geodetic coordinate system, reference point Shaft Monument, with the X axis East, Y axis North, Z axis up, to make a right handed orthogonal system.

POINT NAME	X(+"West") (Meter)	Y(+"Up") (Meter)	Z(+"North") (Meter)
BRASS_1	-0.3794	-3.0428	-28.3462
BRASS_2	-0.4095	-3.6472	-17.5364
BRASS_3	-0.4565	-4.6014	-0.5853
BRASS_4	-0.4992	-5.5025	14.9291
BRASS_5	-0.5917	-7.3838	47.7340
CP_E11	-4.2597	-0.6231	2.3193
CP_E14	-4.2841	-0.9599	7.8030
CP_E17	-4.3020	-1.2735	13.2742
CP_E2	-4.2228	0.2526	-13.5649
CP_E5	-4.2360	-0.0525	-8.0835
CP_E8	-4.2543	-0.3547	-2.6049
CP_W11	4.2588	-0.6368	2.3626
CP_W14	4.2385	-0.9551	7.8415
CP_W17	4.2244	-1.2633	13.3066
CP_W2	4.3026	0.2605	-13.4884
CP_W5	4.2864	-0.0642	-8.0265
CP_W8	4.2681	-0.3728	-2.5563
EI_01	-3.2430	-3.8507	-15.5599
EI_035	-3.2593	-4.1455	-10.4801
EI_065	-3.2502	-4.4319	-5.3970
EI_10	-3.2733	-4.7285	-0.0707
EI_125	-3.2853	-5.0225	5.0019
EI_155	-3.3005	-5.3058	10.0756
EI_18	-3.3291	-5.5984	14.8878
EO_01	-5.9165	-3.7784	-16.7371
EO_09	-5.9821	-4.6861	-0.8124
EO_19	-5.8262	-5.7762	17.9173
PP1	7.2417	-4.2800	21.2850
PP2	7.2279	-4.7573	30.1203
PP3	7.2018	-5.1756	37.2058
VULCAN_E	-4.1054	-2.0351	-8.3983
VULCAN_W	4.1533	-1.8186	-8.1816
WBE_1	-2.7874	-5.9013	20.2109
WBE_1_5	-4.3762	-6.1844	25.2611
WBE_2	-2.8332	-6.4531	29.9410
WBE_2_5	-4.4354	-6.8308	36.5153
WBE_3	-2.9265	-7.1097	41.4054
WBW_1	5.0414	-5.8994	20.2393
WBW_1_5	5.8343	-6.1708	24.8684
WBW_1_7	4.7151	-6.3770	28.4437
WBW_2	5.0588	-6.4587	29.9586
WBW_2_2	4.5839	-6.6437	33.0491
WBW_2_5	5.8101	-6.8466	36.8136
WBW_3	4.9941	-7.1067	41.3270
WI_01	3.3296	-3.8491	-15.5740
WI_035	3.3108	-4.1380	-10.4782
WI_065	3.2895	-4.4296	-5.4146
WI_10	3.2836	-4.7331	-0.0819
WI_125	3.2575	-5.0264	4.9954
WI_155	3.2563	-5.3170	10.0758
WI_18	3.2401	-5.6032	14.9219
WO_01	5.3270	-3.7835	-16.6339
WO_09	5.3542	-4.6834	-0.8288
WO_185	5.3342	-5.6579	15.9071
DetCtr_dsgn	0.0003	0.0075	-0.1307
DetCtr_meas	0.0000	0.0000	0.0000
dcs_origin	0.0431	0.8934	-15.6053
FD_ds_axis	-0.0432	-0.8934	15.6054
FD_us_right	-3.9568	0.8940	-15.6163
FD_us_left	4.0431	0.8927	-15.5944
FD_us_top	0.0431	4.8868	-15.3767
FD_us_bot	0.0431	-3.1001	-15.8340
FD_us_t,r	-3.9568	4.8875	-15.3877

Table 4.6-4. Far Cavern Monuments and Detector Points. In the “Beam” coordinate system with the Z-axis along the beam direction, X-axis horizontal, beam left, and Y-axis to make a right handed orthogonal system.

The line from Fermilab to Soudan is transferred from the surface at Fermilab to underground using conventional survey techniques. The most difficult parameter is the azimuth (horizontal angle). **Table 4.6-5** shows the two methods we are using to determine underground azimuth and the offset (horizontal deviation from the ideal beam line) resulting from the expected angular error at several distances. A gyro-theodolite is a precision theodolite combined with an accurate gyrocompass. One accurate to 15 microradians has been loaned to Fermilab by SLAC and has been in use on NuMI since mid 2001. Both mechanical and optical plumbing is being used down the sight risers and shafts constructed at Fermilab.

Transferring Azimuth	Fermilab Surface to Tunnels				
Method:		Accuracy at:			
	distance >	84 m	460 m	1040 m	735 km
	Accuracy	Downstream	Mid Decay	MINOS	Soudan
	(milliradian)	Target Hall	Tunnel Vent	near det	far det
Best Gyro	0.015	1.3 mm	7 mm	16 mm	11 m
Widely Separated Plumb Bobs	0.012	1.0 mm	6 mm	12 mm	9 m

Table 4.6-5 The two methods being used to determine underground azimuth and the offset (horizontal deviation from the ideal beam line) resulting from the expected angular error at several distances

4.6.3 System Description: Beamline Element Accuracy Requirements

The PBEAM_WMC Monte Carlo was used to calculate the effect of misalignments of each beamline element on the determination of the far detector spectrum (without oscillations) from the measured near detector spectrum. PBEAM is first run with all beam elements at their nominal values and positions ("on axis"). A parameter is selected to investigate and its position is varied from its nominal value. For example, in the Monte Carlo the first focussing horn is moved 4 mm transverse to the beam axis ("Horn 1 X shift of 4 mm"), and the resulting spectra at both near and far detectors are calculated.

The ratio R_{far}, obtained by dividing the far detector flux with the beamline element displaced by the far detector flux with the beamline element on axis, is shown in **Figure 4.6-3a**. A dashed line has been drawn for a flux ratio of 1.0, which would be the result if there were no change in the flux. **Figure 4.6-3b** is a similar graph for the near detector. The ratio of these ratios (far ratio to near ratio, RR) is shown in **Figure 4.6-3c**. It is easy to pick out the largest fractional difference (in the interval 1 to 10 GeV), which occurs near 5 GeV. Beam element misalignments breaking the azimuthal symmetry of the neutrino beam, such as this horn 1 X shift, are measurable in the near detector.

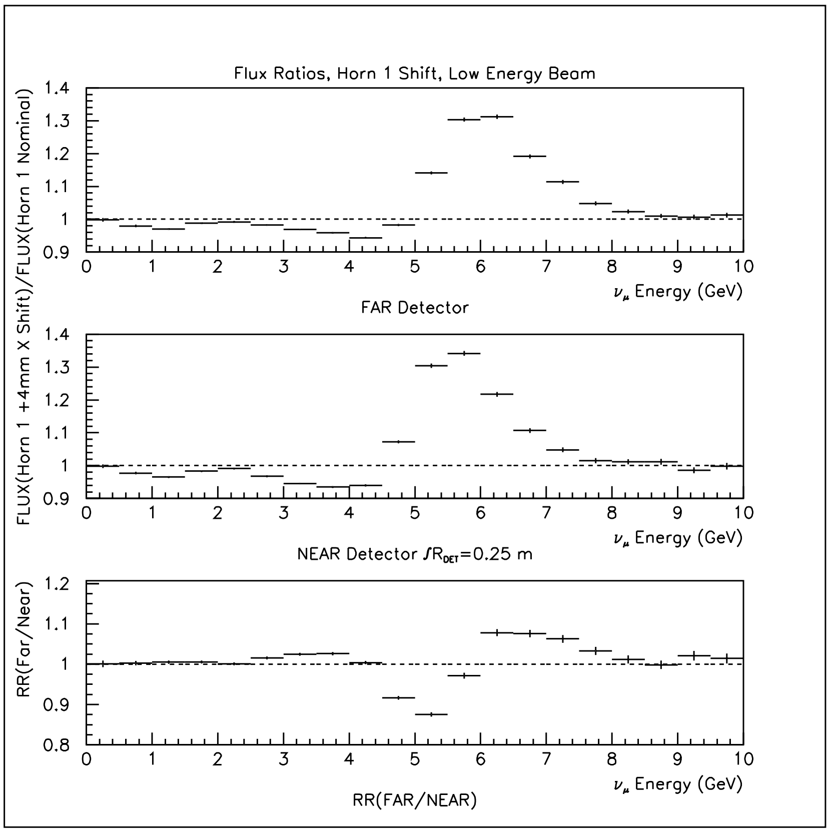

Fig 4.6-3 Effect of a 4 mm offset of horn 1 on (top) the far detector flux, (middle) near detector at 316.6 m beyond the end of the decay pipe, (bottom) far over near ratio(RR). These results are for the low energy beam configuration.

Figure 4.6-4 displays RR-1 for several horn 1 X shifts. These all start at RR-1=0 at low energy, but have been offset by multiples of 10% to clearly display the several curves on a single graph. To obtain sufficient statistical precision from the Monte Carlo in a reasonable time, X shifts much larger than the expected alignment tolerance of 0.35 mm have been calculated. At each peak and valley shown in **Figure 4.6-4**, the data are fit to the formula RR-1=Ax^p. This formula forces the required result of RR=1 at x=0, i.e. no effect on the spectrum if there is no misalignment. The value of RR at the expected alignment tolerance is calculated using the parameters A and p determined by the fit.

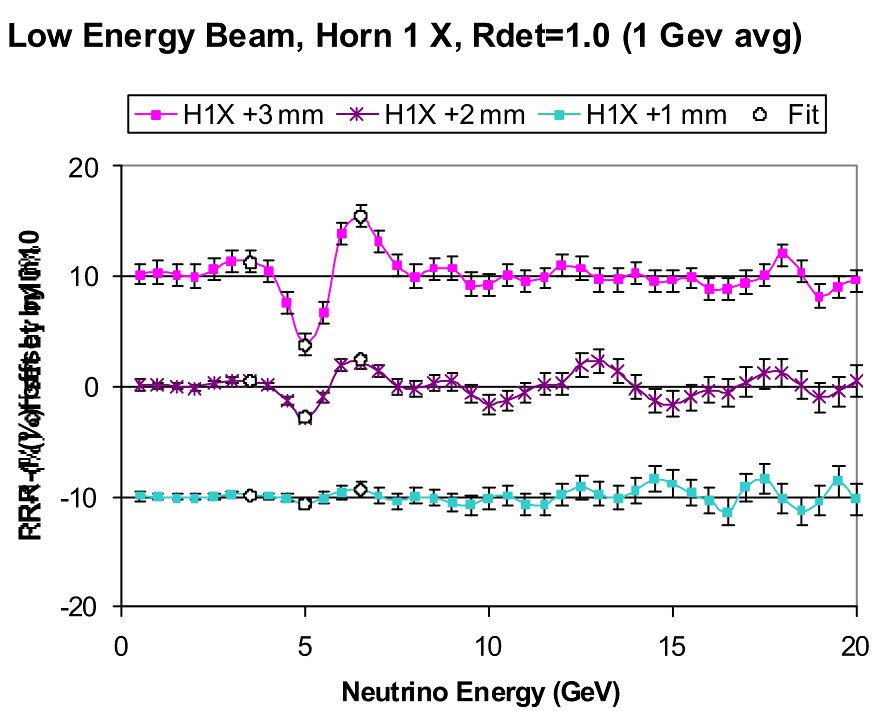

Fig 4.6-4 Curves of RR-1 for several horn 1 X shifts. These all start at RR-1=0 at low energy, but have been offset by multiples of 10% to clearly display the several curves on a single graph. These results are for the low energy beam configuration.

This analysis is repeated for all beam element misalignments shown in **Table 4.6-6**. A similar table is prepared for each 1 GeV neutrino energy interval and, to be conservative, lists the largest deviation of RR found for any neutrino energy up to the table value. The overall effect on RR is found by adding the individual element terms in quadrature. The table takes into account that most misalignments can occur in two transverse planes.

In the table, angle parameters are expressed by a single linear distance; the downstream end of the device is displaced by this amount and the upstream end is displaced by an equal amount in the opposite direction. These two displacements are what are actually measured by the surveyors. The length of the device, in meters, is given in square brackets after the description.

Up to 8 GeV Neutrino Energy							
R=0.25 E	p	A	Misaligned	Expected	Units	(RR-1)exp	Squared
(GeV)		(%)				(%)	(%)2
5.0	2.000	-0.7443	1XP	0.35	mm	-0.091	0.0083
6.0	1.000	0.5864	1AP [3]	0.35	mm	0.205	0.0421
8.0	1.500	-0.4806	2XP	0.35	mm	-0.100	0.0099
6.0	1.000	0.0608	2AP [3]	0.35	mm	0.021	0.0005
5.0	1.500	-0.0272	BAP [10]	0.35	mm	-0.006	0.0000
5.0	1.500	-1.8539	BXP	0.45	mm	-0.554	0.3070<
8.0	1.000	0.9807	TAP [.95]	0.35	mm	0.343	0.1178
8.0	1.000	1.7554	TXP	0.35	mm	0.614	0.3775<<
8.0	1.500	-0.7742	FXP	0.12	100m	-0.032	0.0010
8.0	1.156	1.6285	NXP	0.25	10cm	0.328	0.1076
6.5	1.000	-6.1960	DDM	0.025	m	-0.155	0.0240
7.5	1.000	3.4942	DUM	0.025	m	0.087	0.0076
					Sum		1.0033
					X2		2.0066
					RMS	1.417	
7.0	1.500	0.2646	DRM	2.00	cm	0.748	0.5601<
4.5	1.000	1.2792	HCM	0.50	%	0.640	0.4091
					Sum		2.9758
			All Misalignments:		RMS	1.725	
key:	1st char			2nd char			
	1	horn 1		A	Angle		
	2	horn 2		C	Current		
	B	Beam		D	Downstream		
	D	Decay Pipe X		R	Radius		
	F	Far Det		U	Upstream		
	H	Horns		X	Traverse Offset		
	N	Near Det					
	T	Target		3rd char			
				P	Plus		
				M	Minus		

Table 4.6-6 The expected percentage error in RR from each misalignment at 8 GeV neutrino energy. These results are for the low energy beam configuration

This result is plotted in **Figure 4.6-5** as a function of neutrino energy. Also shown is the statistical error from a two-year run. The MINOS physics requirement is that the error due to neutrino beam misalignments be comfortably below the 2 year run statistical error, and **Figure 4.6-5** shows this to be the case for the low energy beam.

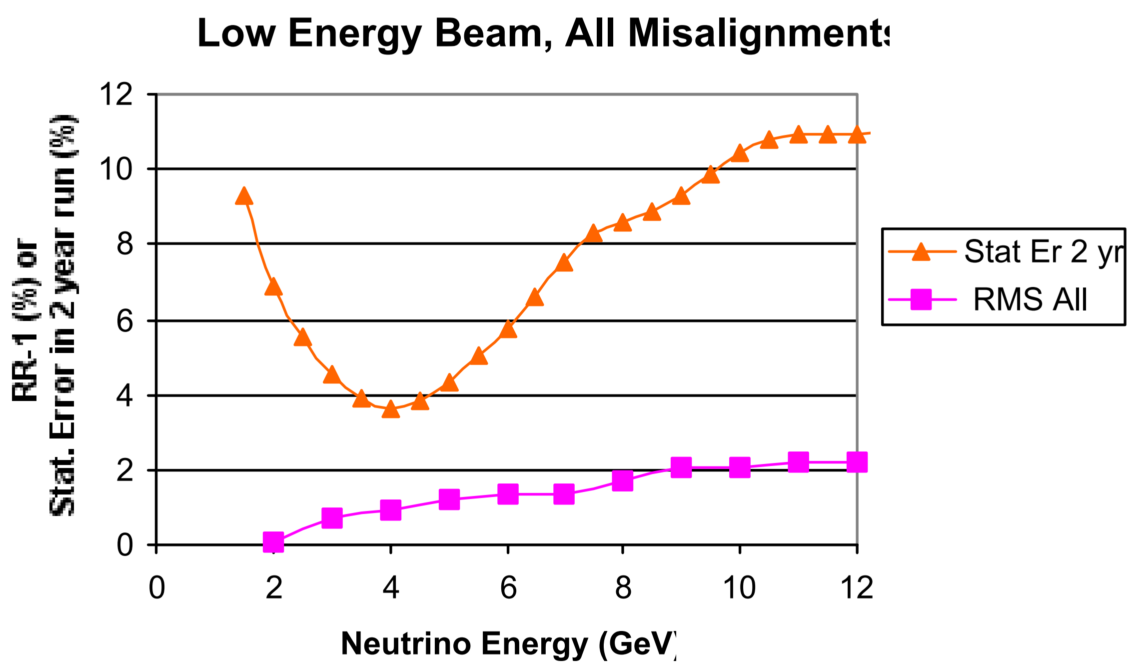

Figure 4.6-5 The expected percentage error in RR from all misalignments listed in **Table 4.6-6**. Also shown is the statistical error for a two-year run. These results are for the low energy beam configuration

4.6.4 System Description: Construction QA

Fermilab surveyors are providing NuMI tunnels and halls quality assurance. Most of the decay tunnel was excavated using a 21.5-foot diameter Tunnel Boring Machine (TBM). **Figure 4.6-6** shows the vertical and horizontal deviations of the center of the TBM decay tunnel from the specified line from Fermilab to Soudan. Measurement of the completed tunnel by both the SA Healy (civil subcontractor) and Fermilab surveyors are shown. Agreement with the design is excellent; most vertical and horizontal centers are within 2 inches. No attempt was made by the two groups of surveyors to measure at the same station (horizontal distance along the tunnel), so local tunnel variations could explain part of the differences between the measurements. The agreement for horizontal is worse than vertical; this is likely conformation that azimuth is the most difficult parameter to transfer underground. The Fermilab surveyors used the 15 microradian gyro-theodolite (0.36 inch in 2000 feet), while the SA Healy surveyors used a less precise 100 microradian instrument (2.4 inch in 2000 feet).

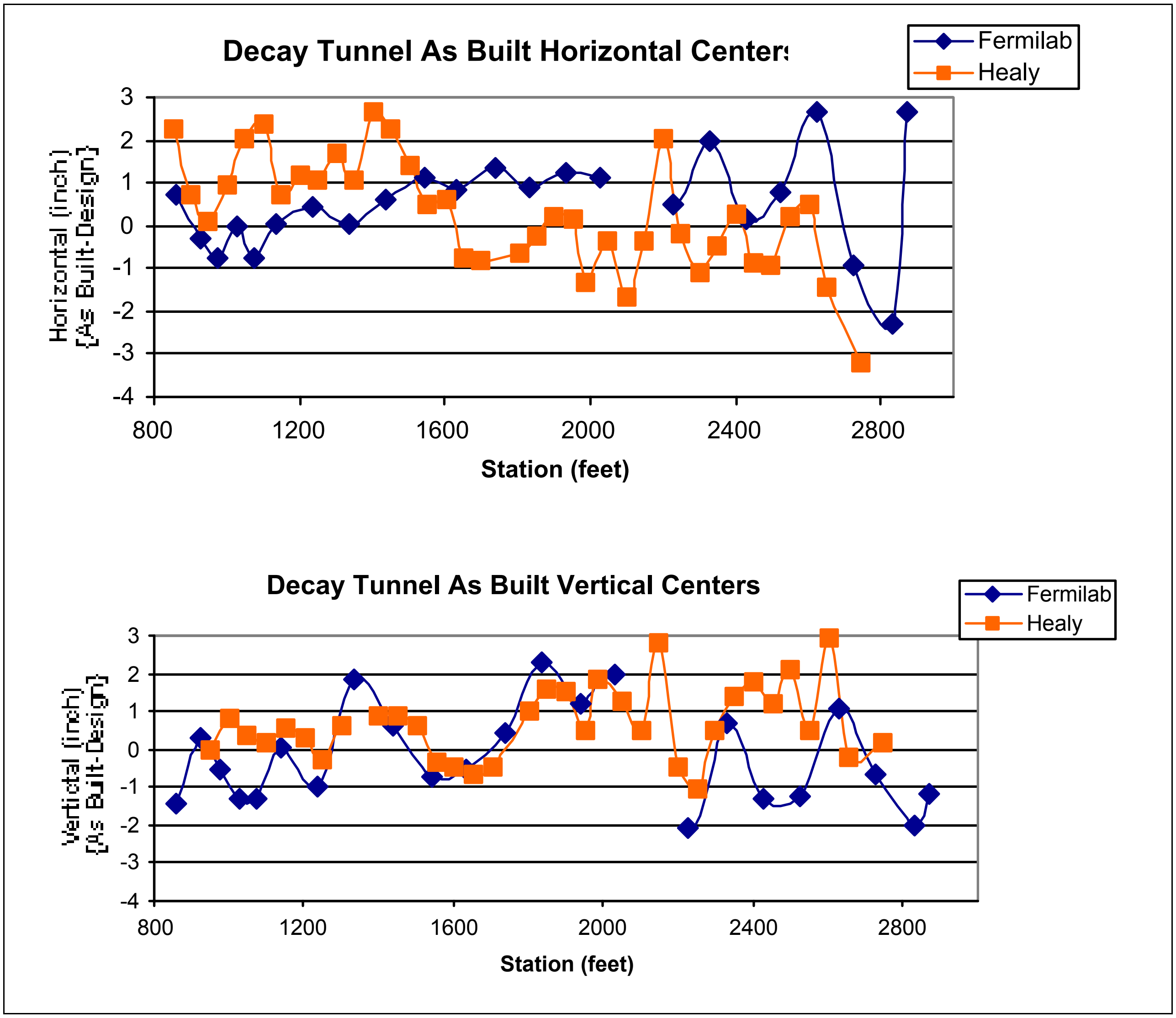

FIgure 4.6-6 The vertical and horizontal deviations of the "as built" center of the TBM decay tunnel from the specification. Measurements of the completed tunnel by both the SA Healy (civil subcontractor) and Fermilab surveyors are shown.